CrossMark

ORIGINAL RESEARCH

Motor Neuron Transdifferentiation of Neural Stem Cell from Adipose-Derived Stem Cell Characterized by Differential Gene Expression

Marzieh Darvishi[1] · Taki Tiraihi[1] · Seyed A. Mesbah-Namin[2] ·
AliReza Delshad[3] · Taher Taheri[4]

Abstract Adipose-derived stem cells (ADSC) are adult stem cells which can be induced into motor neuron-like cells (MNLC) with a preinduction-induction protocol. The purpose of this study is to generate MNLC from neural stem cells (NSC) derived from ADSC. The latter were isolated from the perinephric regions of Sprague–Dawley rats, transdifferentiated into neurospheres (NS) using B27, EGF, and bFGF. After generating NSC from the NS, they induced into MNLC by treating them with Shh and RA, then with GDNF, CNTF, BDNF, and NT-3. The ADSC lineage was evaluated by its mesodermal differentiation and was characterized by immunostaining with CD90, CD105, CD49d, CD106, CD31, CD45, and stemness genes (Oct4, Nanog, and Sox2). The NS and the NSC were evaluated by immunostaining with nestin, NF68, and Neurod1, while the MNLC were evaluated by ISLET1, Olig2, and HB9 genes. The efficiency of MNLC generation was more than 95 ± 1.4 % (mean $\pm$ SEM). The in vitro generated myotubes were innervated by the MNLC. The induced ADSC adopted multipolar motor neuron morphology, and they expressed ISLET1, Olig2, and HB9. We conclude that ADSC can be induced into motor neuron phenotype with high efficiency, associated with differential expression of the motor neuron gene. The release of MNLC synaptic vesicles was demonstrated by FM1-43, and they were immunostained with synaptophysin. This activity was correlated with the intracellular calcium ion shift and membrane depolarization upon stimulation as was demonstrated by the calcium indicator and the voltage-sensitive dye, respectively.

Keywords Stem cell · ADSC · Motor neurons · Transdifferentiation · Induction

Introduction

It was suggested that medical techniques may someday make use of the potential shown by transdifferentiation of somatic cells (Mirakhori et al. 2014), Krabbe et al. (2005) suggested the use of the transdifferentiated mesenchymal stem cells as a source for cell therapy in neurodegenerative diseases, such as amyotrophic lateral sclerosis (ALS), which is characterized by degeneration of motor neurons (Silani et al. 2002). The experimental work on the ALS mouse model showed that transplantation of human motor neurons generated from neural stem cells delayed clinical onset and prolonged the animal life (Lee et al. 2014). Motor neurons can be generated from several sources such as embryonic stem cells (ESCs) and induced pluripotent stem cells (iPSC) (Nizzardo et al. 2010). Transdifferentiation of adipose derive stem cells (ADSC) was suggested as a source for the neural lineage in cell therapy (Kokai et al. 2005), because they are autologous and can be easily obtained and transdifferentiated into motor neuron-like cells (MNLC). In vitro differentiated neurons showed immunostaining of their processes with synaptophysin; moreover, they could load and unload FM1-43

✉ Taki Tiraihi
takialtr@modares.ac.ir; ttiraihi@hotmail.com

[1] Department of Anatomical Sciences, Faculty of Medical Sciences, Tarbiat Modares University, P.O. Box 14155-4838, Tehran, Iran

[2] Department of Clinical Biochemistry, Faculty of Medical Sciences, Tarbiat Modares University, Tehran, Iran

[3] Department of Anatomy, Shahed University, Tehran, Iran

[4] Shefa Neurosciences Research Center, Khatam Al-Anbia Hospital, Tehran, Iran

Springer

fluorochrome (Bieberich and Anthony 2004). Similar results were reported in transdifferentiating bone marrow stromal cells into GABAergic neurons (Mohammad-Gharibani et al. 2012), and others confirmed the release of synaptophysin immunoreactive synaptic vesicles from transdifferentiated ADSC (Cardozo et al. 2010). The in vitro morphology of the transdifferentiated cells showed multipolarity with several cytoplasmic processes originated from the MNLC and contacted the myotubes using a co-culturing system (Abdanipour and Tiraihi 2012).

Differential gene expression (Shh and BMP) was reported in transdifferentiating ADSC into neuronal phenotype, and both genes were involved in cell fate determination and proliferation (Cardozo et al. 2010). In a previous study, we reported induction of ADSC into MNLC with an efficiency of 76 %, and it was characterized by differential patterning in ISLET1, Olig2, and HB9 expression during the transdifferentiation with shifting gene expression at the early stage of induction (Abdanipour and Tiraihi 2012).

The purpose of this study is to transdifferentiate ADSC into NSC and use them in generating MNLC in order to improve the yield, which can be used for cell therapy in motor neuron degenerative disorders. The evaluation of the in vitro activity of MNLC was demonstrated by the voltage-sensitive dye (VSD) so as to probe the membrane characteristics, show synaptic release using FM1-43, and demonstrate intracellular calcium ion shift using Fluo-4 NW. Moreover, the functional morphology of MNLC was also assessed by co-culturing them with myotubes, while the molecular analysis confirmed the differentiating motor neuron gene expression.

Materials and Methods

The production of MNLC was achieved by converting the ADSC into NS, which were then used for generating NSC, and these were induced into MNLC.

Rat ADSC Isolation and Characterization

The ADSC were isolated from 5 female Sprague-Daley rats (6–8 weeks old) purchased from Razi Institute, Tehran, Iran. The experiments were approved by the ethical committee of the Faculty of Medical Sciences at Tarbiat Modares University and were done according to Helsinki guidelines for the laboratory animal use. The isolation of the ADSC was done according to a previous investigation (Abdanipour and Tiraihi 2012): the sampled adipose tissue was incubated in a DMEM containing 0.075 % collagenase type I (Sigma-Aldrich, Steinheim, Germany) for 30–50 min at 37 °C with agitation, and then it was

neutralized with 10 % fetal bovine serum (FBS: GIBCO-BRL, Eggenstein, Germany), filtered through 100-μm mesh cell strainers (BD Biosciences, Stockholm, Sweden), and centrifuged at 1200 rpm for 10 min. The precipitate was cultured in a T25 flask containing DMEM with 10 % FBS and penicillin–streptomycin, incubated at 37 °C with 5 % CO_2 in a humidified incubator for 24 h, washed twice with PBS, harvested with trypsin/EDTA (0.05 % trypsin/0.5 mM EDTA: GIBCO-BRL, Eggenstein, Germany), and cultured for 3 passages, respectively. The osteogenesis and lipogenesis of ADSC were done according to a previous report (Darabi et al. 2013). Briefly, the lipogenic differentiation was performed by incubating ADSC at the third passage with an adipogenic induction medium containing 50 μg/ml indomethacin, 50 μg/ml ascorbic acid, and 100 nM dexamethasone (Sigma-Aldrich, Steinheim, Germany). After 3 weeks, the lipid vacuoles were stained with Oil Red O (Sigma-Aldrich), whereas the osteogenic induction was carried out by incubating the ADSC of the third passage with an osteogenic induction medium containing 10 mM β-glycerophosphate, 60 μM ascorbic acid, and 0.1 μM dexamethasone (Sigma-Aldrich, Steinheim, Germany). The calcium deposits and the osteogenic differentiation were identified by Alizarin Red S staining (Sigma-Aldrich, Steinheim, Germany). The chondrogenic differentiation was done by incubating the ADSC of the third passage with chondrogenic induction medium containing 6.25 μg/ml insulin, 6.25 μg/ml transferrin, 1.25 μg/ml bovine serum albumin (BSA), 50 μg/ml ascorbic acid, 10^{-7} M dexamethasone, and 10 ng/ml TGF-β3 (Sigma-Aldrich, Steinheim, Germany), and the chondrogenesis was assessed by Safranin O stain (Baptista et al. 2013).

The isolated ADSC at the 3rd passage were cultured on a 6-well plate for immunostaining with the primary antibodies against CD90, CD105, CD49d, CD106, CD34, CD31, and CD45 (see Table 1), and the immunolabeling was done according to the immunocytochemistry section below.

Conversion of Rat ADSC into Neurospheres (NS)

The ADSC of the 5th passage were harvested using trypsin/EDTA and plated on a six-well culture plate at a density of 5×10^5 cell/ml with 2 ml of neurosphere medium (NM: consisted of serum-free DMEM/F12 containing 2 % B27 supplement, 20 ng/ml the epidermal growth factor (EGF), and 20 ng/ml the basic fibroblast growth factor (bFGF); all purchased from Invitrogen, Paisley, Scotland). The cell aggregates forming the NS were evaluated after 3 days, while a fresh NM was added every day for 1 week (Darabi et al. 2013). Then the NS was cultured on poly-L-lysine (Sigma-Aldrich, Steinheim, Germany) coated cover slips inside a 12-well plate containing NM, incubated in a

humidified incubator with 5 % CO_2 at 37 °C for 2 h, fixed with 4 % formaldehyde (Sigma-Aldrich, Steinheim, Germany) for 20 min, permeabilized with 0.1 % Triton X-100 (Sigma-Aldrich, Steinheim, Germany), labeled with the primary antibodies (nestin, neurofilament 68 (NF68), Sox2, Oct4, and Nanog) overnight at 4 °C, washed with PBS three times, incubated with the secondary antibodies for 2 h at room temperature, counterstained with propidium iodide (PI), and examined with a fluorescence microscopy (Olympus IX71: Olympus, Japan) at 200× magnification, respectively (Darabi et al. 2013).

The ADSC of the fifth passage used as a control were incubated for 10 days with DMEM supplemented with 10 % FBS and penicillin–streptomycin, and were immunostained as above. The positive control was a neonate rat brain.

Neural Stem Cell (NSC) Generation from Neurospheres (NS)

After 7 days, the NS were harvested into single cells using accutase (Invitrogen, Eggenstein, Germany), and then the dissociated cells were seeded on a T25 flask (2×10^6-density) in NM supplemented with 10 % FBS (NSC culture medium). The cells were maintained in a humidified incubator with 5 % CO_2 at 37 °C, while the medium was changed every day for 10 days (Darabi et al. 2013). The NSC were cultured on a 6-well plate and immunolabeled with antibodies against Sox2, Oct4, nestin, NF68, NF160, Map2, and Neun. Also, they were evaluated with the RT-PCR technique for Oct4, Nanog, and Sox2 genes.

The ADSC of the fifth passage were used as a control, and they were incubated for 10 days with DMEM supplemented with 10 % FBS and penicillin–streptomycin and immunostained as above. The positive control was a neonate rat brain.

Induction of NSC into Motor Neuron-Like Cell (MNLC)

The NS-derived NSC were seeded in a T25 flask at 1×10^6 density (50 % confluency) and incubated in an NM containing RA (0.1 M: Sigma-Aldrich, Steinheim, Germany) and Shh (1 μg/ml: Invitrogen, Paisley, Scotland), and the medium was replaced every day. After 5 days, the brain-derived neurotrophic factor (BDNF), the glial-derived neurotrophic factor (GDNF) (each 10 ng/ml: Invitrogen, Paisley, Scotland), the ciliary neurotrophic factor (CNTF), and neurotrophin 3 (NT-3) (each 5 ng/ml: Invitrogen, Paisley, Scotland) were added to the culture medium, which was replaced every day for 7 days. Immunostaining for ISLET1, Olig2, HB9, Chat, and Map2 markers was applied for evaluating the MNLC. The RT-PCR technique was used in evaluating ISLET1, Olig2, and HB9 in MNLC.

The efficiency of MNLC transdifferentiation was calculated from this equation:

$$\text{efficiency} = (\text{MNLC yield} \times \text{ADSC viability}) \times 100.$$

The yield of MNLC was 97 % (the percentage of immunoreactive cells to Hb9), and the viability of ADSC was 98 %, and therefore, the efficiency was 95.06 %, and if we entered the three replicate of MNLC yield, the results will be 95.06 ± 1.4 % (mean $\pm$ SEM).

Two control groups were used: the first group was ADSC cultured for two weeks with DMEM supplemented with 10 % FBS and penicillin–streptomycin, and immunostained as above. The other control was NSC cultured for the same period and treated with the NSC culture medium, both controls were immunostained as above. The positive control was a neonate rat spinal cord.

Immunocytochemistry

The cells were cultured on a six-well plate, washed with PBS, fixed in 4 % paraformaldehyde for 30 min, and then permeated and blocked with 0.3 % Triton X-100 and 5 % FBS for 20–25 min. The ADSC were incubated with the primary antibodies (see Table 1) overnight at 4 °C, washed three times in buffer, and incubated with the relevant secondary antibody for 2 h at room temperature. After three washes, the samples were counterstained with propidium iodide (PI) and visualized at 200× magnification (Olympus IX71: Olympus, Japan) (Darabi et al. 2013). The negative control was done on cells incubated with the secondary antibodies without the primary ones.

The percentage of the immunoreactive cells was obtained by dividing the number of the immunoreactive cells to the total number of cells in at least five random fields, where 500 cells were counted in three independent cultures according to Naghdi et al. (2009), and the immunolabeling was repeated three times.

RT-PCR

The expression of Oct4, Nanog, Sox2, and nestin in the NSC as well as Olig2, ISLET1, and HB9 genes in the NSC, the MNLC, and the newborn spinal cord (positive control) were evaluated by using the reverse transcription polymerase chain reaction (RT-PCR) technique. In this method, the total RNA was extracted from the control and the experimental samples by AMBION kit (Invitrogen, Paisley, Scotland). The cDNA was synthesized using the oligo-dT primer and amplified by 35 cycles in a thermocycler using the primer sets listed in Table 2. The primer

Table 1 Primary antibodies used in the immunocytochemical evaluation of the adipose-derived stem cells (ADSC), the neurospheres (NS), the neural stem cells (NSC), and the motor neuron-like cells (MNLC)

Primary Antibody Anti-	P/M[a]	host	titer	Labeled cells	Source (company)	Secondary antibody
CD105	M	Mouse	1:200	ADSC	Millipore[b]	R
CD49d	P	Rabbit	1:300	ADSC	Millipore[b]	G
CD106	M	Mouse	1:300	ADSC	Millipore[b]	R
CD31	M	Mouse	1:300	ADSC	Millipore[b]	R
CD45	P	Rabbit	1:300	ADSC	Millipore[b]	G
CD34	P	Goat	1:500	ADSC	R&D Systems[b]	R
CD90	M	Mouse	1:300	ADSC	Millipore[b]	R
Nestin	M	Mouse	1:100	NSC,NS,MNLC	Millipore[b]	R
NF68	M	Mouse	1:200	NSC,NS,MNLC	Millipore[b]	R
NF 160	M	Mouse	1:200	NSC,NS,MNLC	Millipore[b]	R
Neun	M	Mouse	1:200	NSC,NS,MNLC	Millipore[b]	R
Neurod1	M	Mouse	1:200	NSC,NS,MNLC	Millipore[b]	R
Chat	M	Mouse	1:200	NSC,NS,MNLC	Millipore[b]	R
Map2	P	Rabbit	1:200	NSC,NS,MNLC	abcam[b]	G
Oct4	P	Rabbit	1:200	NSC,NS,MNLC	abcam[b]	G
Sox2	P	Rabbit	1:200	NSC,NS,MNLC	abcam[b]	G
Nanog	P	Rabbit	1:200	NSC,NS,MNLC	abcam[b]	G
ISLET1	P	Rabbit	1:200	NSC,NS,MNLC	abcam[b]	G
Olig2	P	Rabbit	1:200	NSC,NS,MNLC	abcam[b]	G
HB9	P	Rabbit	1:200	NSC,NS,MNLC	abcam[b]	G

The secondary antibodies were either rabbit anti-mouse FITC-conjugated (R) or goat anti-rabbit FITC-conjugated (G) (abcam, Cambridge, UK); the titers of both secondary antibodies were 1:500

[a] P/M represents either polyclonal or monoclonal, respectively

[b] Represents the source of antibodies either Millipore, Schwalbach, Germany, R&D systems, Wiesbaden, Germany, or abcam, Cambridge, UK.

Table 2 Presents the genes used in the molecular evaluation of the neural stem cells and motor neuron-like cells, the accession number, the forward and backward primers, and the polymerized DNA segment size (bp)

Gene	Accession No.	Forward	Reverse	Size bp
ISLET1	NM_017339.3	CACACTCGGATGACTCTGG	CTTGCGGACCTGGTATGC	99
Olig2	NM_001100557.1	CCAGCAACAATTAACTTAGG	CTTAGAAGAGACGCAGAG	155
HB9	NW_001084822	ATGAGGATGAGGATGATGAAGAAG	CAGATGAGCAATCGGATGAGG	138
Oct4	NM_031068.1	GGCTGTGTCCTTTCCTCT	TCTCTTTGTCTACCTCCCTTC	217
Nanog	NM_001100781.1	TTCAAGACCAGCCTGTACT	GCACTGGTTTATCATGGTAC	220
Sox2	NM_001109181.1	CCGTTACAGACAAGGAAGG	CAACGATATCAACCTGCATG	195
Nestin	NM_012987.1	AAGGCTCAGGAGTTCCAGG	TACGGCTTTATTCAGGGAG	245
GAPDH[a]	NM_002046.3	CAAGGTCATCCATGACAACTTTG	GTCCACCACCCTGTTGCTGTAG	496
GAPDH[b]	NM_002046.3	GTTGTCTCCTGCGACTTCA	GGTGGTCCAGGGTTTCTTA	190

[a] Used in electropherogram Fig. 4B

[a] Used in electropherogram Fig. 2R

sequences were designed with the Primer Design software (primer 3 plus: www.bioinformatics.nl/primer3plus/) and then controlled by the Gene Runner software (version 3.05; Hastings Software Inc., Hastings, NY, USA: http://www. generunner.com). The house-keeping gene (GAPDH) was used as an internal control. The PCR product was electrophoresed using 1 % agarose and stained with GelRed (Invitrogen, Karlsruhe, Germany). The DNA bands were

observed and photographed with a gel documentation system (Uvtec, Cambridge, UK). This technique was repeated three times (Darabi et al. 2013).

Co-culturing with Myotube

In order to evaluate the in vitro activity of the generated MNLC, they were cultured with myotubes (derived from mouse muscle cell line (C2C12 myoblasts): American Type Culture Collection, Rockville, Md, USA) (Hester et al. 2011). They were cultured with DMEM containing 10 % FBS on cover slips, and they grew to confluency, while the medium was replaced with DMEM containing 10 % horse serum (Invitrogen, Paisley, Scotland) for 3–7 days. The myotubes were used for co-culturing experiments 4 days following differentiation, while the cells were stained with Cresyl violet stain (Abdanipour and Tiraihi 2012).

Analysis of MNLC Synaptic Release Rate

The in vitro MNLC activity was evaluated with synaptic vesicle release upon stimulation, the MNLC were seeded in 24-well plates at 6×10^3 density. The lipophilic fluorochrome (FM1-43: Molecular Probes, Leiden, The Netherlands) for imaging vesicle recycling was assessed using an inverted epifluorescence microscope (Olympus IX71: Olympus, Japan). The MNLC were washed and left for 10 min in a saline containing 170 mM NaCl, 3.5 mM KCl, 0.4 mM KH_2PO_4, 5 mM $NaHCO_3$, 1.2 mM Na_2SO_4, 1.2 mM $MgCl_2$, 1.3 mM $CaCl_2$, 5 mM glucose, and 20 mM tris (hydroxymethyl)-methyl-2-aminoethanesulfonic acid. The solution was replaced with stimulating solution 1 containing saline supplemented with 100 mM KCl and 10 μM FM1-43 for 2 min, and then the solution was removed and replaced with stimulating solution 2 containing 3.5 mM KCl and 10 μM FM1-43 for 3 min, and this was repeated three times. For unloading the dye, the solution was changed with a saline containing 100 mM KCl, and the dye unloading was visualized using an inverted epifluorescence microscope (10 min with a photograph each min) (Gharibani et al. 2010).

Ca^{2+} Influx Imaging

The shift in the intracellular Ca^{2+} of the MNLC (cultured on 24-well plates at 6×10^3 density) following stimulation was determined with a fluorescent Ca^{2+} indicator (Fluo-4 NW: Molecular Probes, Leiden, The Netherlands). The MNLC were cultured in a medium containing 5 % FBS for 3–4 days, which was removed, and 0.5 ml of the fluorochrome loaded solution (Fluo-4 NW solution: 1 mM) was added to each well plate. The plates were incubated at

37 °C for 20 min, and then the Fluo-4 NW was removed, and the cells were washed once with the HEPES and incubated for 1 h (Dawitz et al. 2011).

Voltage-Sensitive Dye (VSD) Imaging

For loading RH795 (Molecular Probes, Leiden, The Netherlands) in the MNLC, the medium was replaced with 20 μl of the dye loading solution (RH795 solution: 20 mg/ml) in artificial cerebrospinal fluid (ACSF: 119 NaCl, 26 $NaHCO_3$, 10 glucose, 2.5 KCl, 1 NaH_2PO_4, 1.5 $MgSO_4$, and 1.5 $CaCl_2$). The cells were incubated at 37 °C in the dark, washed 3 times, incubated for 60 min with the ACSF in the dark, and examined using inverted epifluorescence microscope, respectively (Olympus IX71: Olympus, Japan). The RH795 was excited by instrument settings appropriate for excitation at 380 nm (calcium free) and 340 nm (calcium complex) with fixed emission at 510 nm (Canepari and Zecevic 2010).

Statistical Analysis

The ANOVA with Tukey's multiple comparison was used in evaluating the results using SPSS 10 (SPSS Inc., Chicago, IL).

Results

Rat ADSC Isolation and Characterization

The isolated ADSC at the fourth passage became more homogenous compared with the primary culture and the first passage (Fig. 1A–C). The lipogenic, osteogenic, and chondrogenic differentiation of the ADSC was noticed (see Fig. 1D–F), and they were characterized by immunoreactivity to the markers CD90 (mesenchymal stem cell marker), CD105 (fat-derived mesenchymal stem cell marker), and CD49d (fat cell specific marker), see Fig. 1G–I, while they showed negative immunostaining to CD106 (mesenchymal stem cells derived from the bone marrow stromal cell marker), CD31 (endothelial cell marker), and CD45 (hematopoietic stem cell marker), see Fig. 1J–L. The ADSC cultures were positive for CD90, CD105, and CD49d with PIC > 95 % and negative for CD31, CD34, CD45, and CD106 with PIC < 10 %.

ADSC Conversion into NS and NSC Generation

The floated NS are presented in Fig. 2A–C, whereas the morphology of the NSC derived from the NS is presented in Fig. 2D. Characterization of the NS was done by immunostaining with nestin (NSC marker), neurofilament
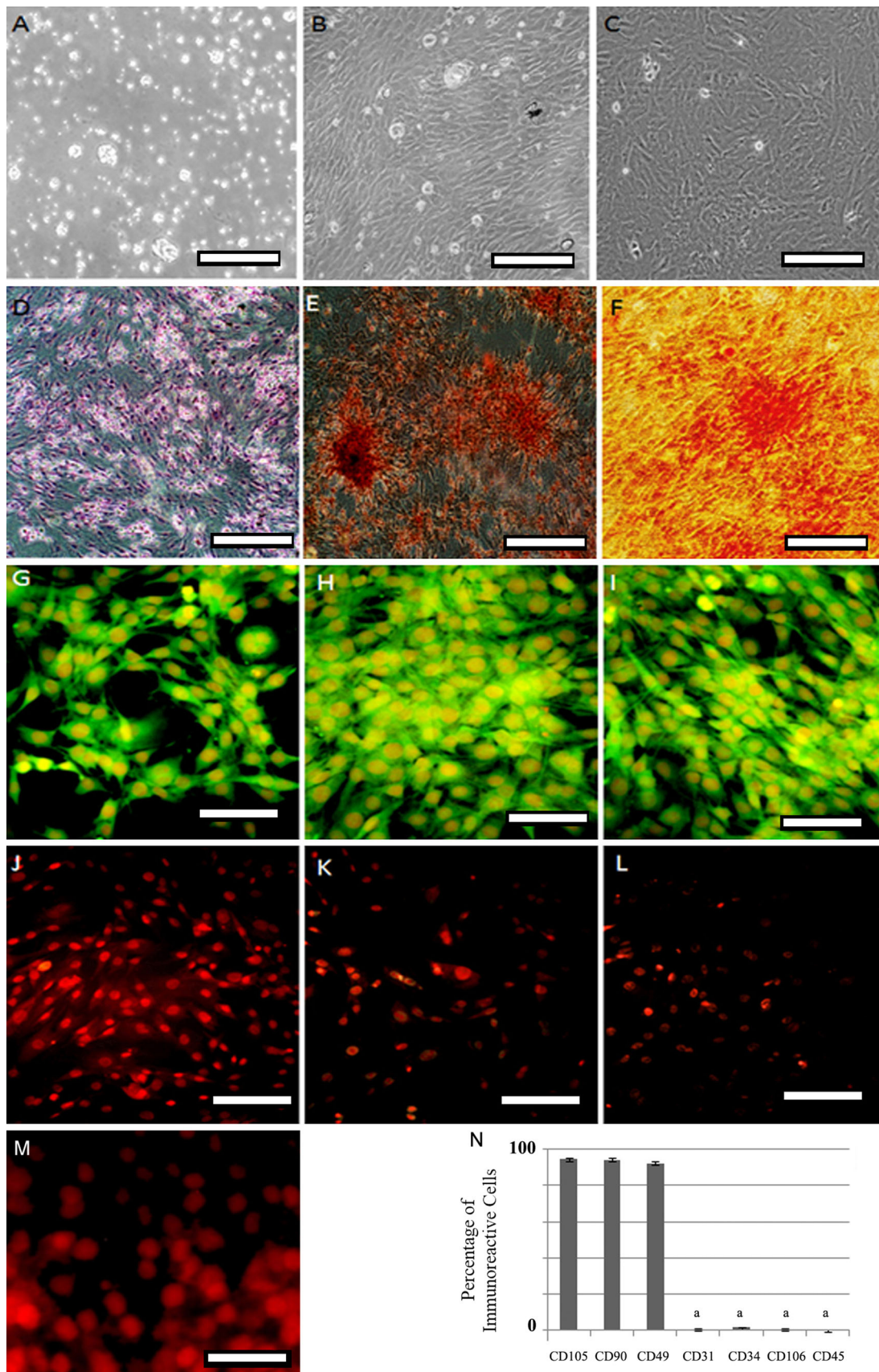
◄**Fig. 1** Cultured adipose-derived stem cells (ADSC), mesenchymal differentiation lineage, immunostaining, and the percentage of immunoreactive cells to *each marker*. **A–C** Phase contrast images of the primary culture of the ADSC (24 h), the first passage of the cultured ADSC (5 days), and the fourth passage of the culture (14 days), respectively. **D** Lipogenic differentiation of the cultured ADSC forming multilocular fat cells stained with Oil red stain. **E** Osteogenic differentiation of the cultured ADSC forming bone ossicle stained with Alizarin red stain. **F** Chondrogenic differentiation of the cultured ADSC extracellular matrix stained with safranin O stain. **G–I** Immunolabeling with the primary antibodies to CD90, CD105, and CD49d, respectively; they were incubated with a secondary antibody conjugated with FITC and counterstained with propidium iodide. **J–L** Immunolabeling with the primary antibodies to CD106, CD31, and CD45, respectively; they were incubated with the secondary antibody conjugated with FITC and counter stained with propidium iodide. **M** Histogram of the percentages of immunoreactive cells (ADSC) to CD105, CD90, CD49d, CD31, CD106, and CD45. *a* Statistically different from CD105, CD90, and CD49d. *scale bar*: **A–F** = 200 μm, **G–L** = 50 μm and **M** = 25 μm)

68 (NF68: undifferentiated neuron marker), Sox2, Oct4, and Nanog (markers for stemness; Fig. 2E–I, respectively).

The NSC were immunoreactive to Sox2, Oct4, nestin, NF68, and NF160 (differentiating neuronal markers) (Fig. 2J, K, M, N, and O, respectively). They were negatively immunostained with Map2, Neun, and Neurod1 (differentiated neuron markers) (Fig. 2L, P, Q, respectively). The expressions of NF68 and Neurod1 (a marker of NSC) was significantly higher than those of Map2 and Neun ($P < 0.05$). Also, the expressions of Sox2 and Oct4 were significantly higher than those of Map2 and Neun ($P < 0.05$), whereas that of CD106 was significantly lower than those of CD105 and CD49d (Fig. 2R). The RT-PCR results of Oct4, Nanog, Sox2, and nestin genes are consistent with their immunostaining.

Induction of NSC into MNLC

Figure 3 represents the immunostaining of the induced NSC into MNLC at 1, 2, and 14 days using anti-Olig2 (motor neuron progenitor marker), anti-ISLET1 (motor neuron precursor marker), anti-HB9 (marker for differentiated motor neurons), anti-Chat (marker for cholinergic neurons), and anti-Map2 (neuronal marker). There was noticeable gradual increase in the expression of HB9 in the differentiating MNLC, and a similar pattern was noticed in the expression of Chat. The PIC of Olig2 at day 1 was higher than the other time points; while the highest percentage of ISLET1 was at day 2, the highest percentages of HB9, Map2, and Chat were at the second week ($P < 0.05$) (Fig. 4A). Moreover, the results of the RT-PCR show that HB9, Olig2, and ISLET1 were expressed in the MNLC (See Fig. 4B).

Co-culture of MNLC with Myotubes

The co-culturing of the myotubes and the differentiated MNLC is presented in Fig. 4C–F, where the MNLC extensions can be seen in direct contacts with the myotubes resulting in in vitro innervation of the myotubes, while the morphology of MNLC shows typical multipolar cell contact with the myotubes (Fig. 4E, F).

Vesicle Release from MNLC

Figure 5A–C demonstrates an in vitro preparation of MNLC stained and destained with fluorescent lipophilic fluorochrome (FM1–43), and the results show that they had labeled the synaptic vesicles with fluorochrome, the synaptic vesicles destained following stimulation (Fig. 5B, C). The synaptic vesicles turnover during the stimulation demonstrates a monoexponential decay model ($y = 64.15e^{-0.14t}$) (Fig. 5D). After double labeling the differentiated cells with FM1-43 and synaptophysin, the immunocytochemistry shows that these vesicles (stained with FM1-43) were immunostained with synaptophysin, while they were labeled with FM1-43 (Fig. 5E), where many of the vesicles were located at the contact sites with the other cells.

Ca²⁺ Concentration Influx Shift

Figure 6 demonstrates the staining of MNLC with Fluo-4 NW, Ca^{2+} indicator, and the images were taken serially, and they showed gradual changes in the image color depending on the intracellular Ca^{2+} concentration shift from low to high.

Voltage-Sensitive Dye (VSD) Imaging

The staining with VSD (RH795) is presented in Fig. 7, and the red color (F) represents a depolarized membrane resulted from action potential excitation, while the shift in the color indicates the repolarization of the excited membrane.

Discussion

The ADSC immunostaining results showed the cells were immunoreactive to ADSC markers (CD90, CD105 and CD49d), while they were negatively immunostained to hematopoietic (CD34 and CD45) and endothelial cell markers (CD31). The results of this investigation show that MNLC can transdifferentiate from ADSC-derived NSC with high efficiency. The main feature of MNLC is their ability to form cell to cell contact with the myotubes in an
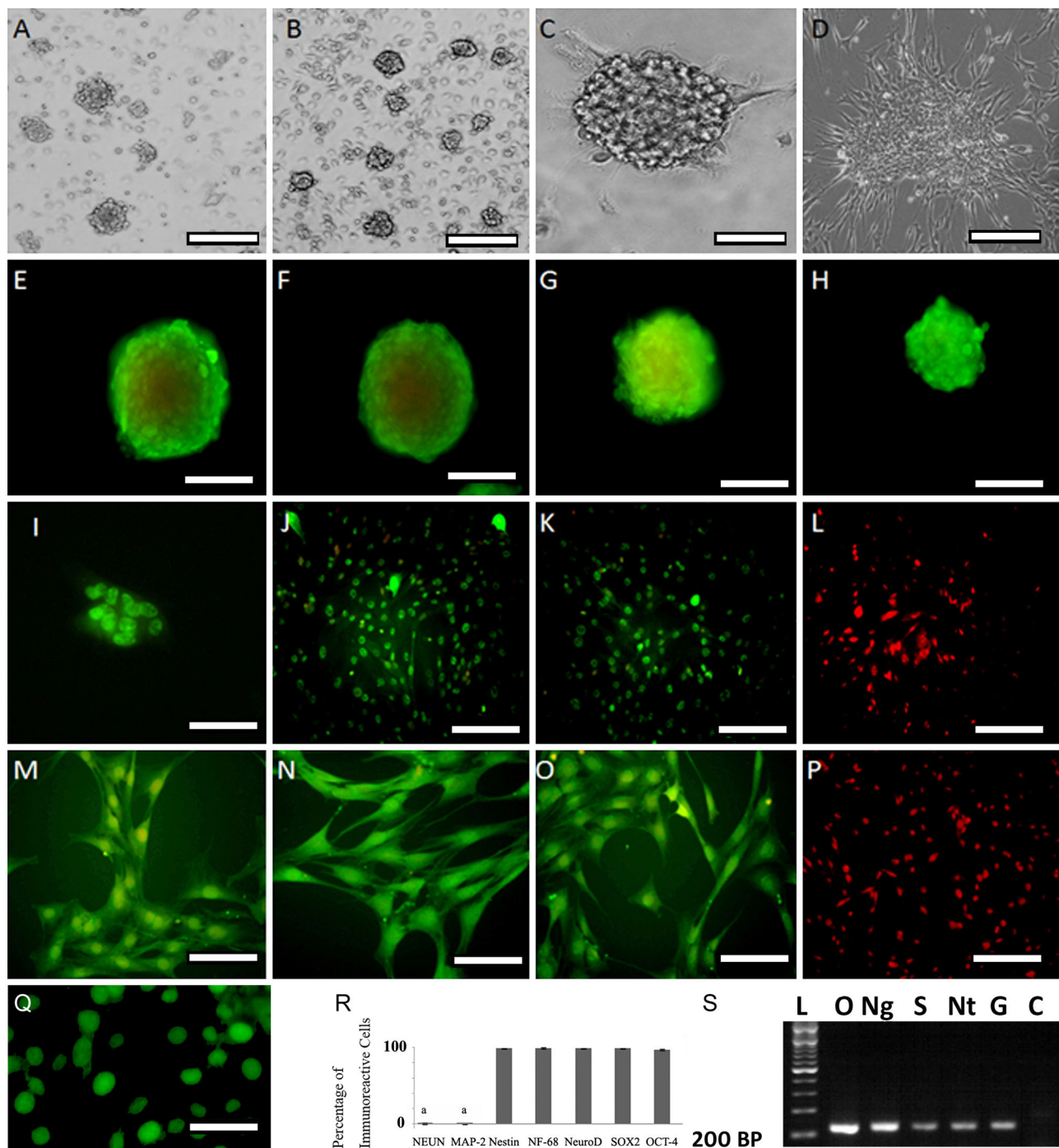
Fig. 2 Morphology of the neurospheres (NS), the neural stem cells (NSC) immunostained with different markers, the percentage of immunoreactive cells to each marker, and the electrophoresis results of the reverse transcription polymerase chain reaction (RT-PCR) of NSC. **A–C** Phase contrast images of the NS at 1, 2, and 7 days, respectively. **D** Phase contrast image of NSC generated from the NS. **E–I** Immunolabeling of the NS with the primary antibodies (Nestin, neurofilament 68, Sox2, Oct4 and Nanog, respectively) followed by a relevant secondary antibody conjugated with FITC, and **E** and **F** Counterstained with propidium iodide. **J–Q** Immunolabeling of NSC with the primary antibodies Sox2, Oct4, Map2, nestin, NF-68, NF-160, Neun, and Neurod1, respectively, followed by a relevant secondary antibody conjugated with FITC and counterstained with propidium iodide (only Map2, nestin, NF-68, and NF-160 were counterstained with propidium iodide). **R** Histogram of the percentage of immunoreactive cells (NSC) to Map2, Neun, nestin, neurofilament 68, Neurod1, Sox2, and Oct4. *a* Statistically different from nestin, NF68, Neurod1, Sox2, and Oct4. **S** Electropherogram of RT-PCR of NSC, the lanes of RT-PCR for Oct4 (O), Nanog (Ng), Sox2 (S), nestin (Nt), G (glyceraldehyde 3-phosphate dehydrogenase, GAPDH: house-keeping gene as an internal control), C (no template control: NTC), and L (DNA ladder) (*scale bar* **A–C** = 100 μm, **D** = 200 μm, **E–I** = 100 μm, **J–L** = 200 μm, **M–O** = 50 μm, **P** = 200 μm and **Q** = 25 μm)

Fig. 3 Immunostaining of the motor neuron-like cells (MNLC) with the primary antibodies at day 1, day 2, and two weeks, respectively. The MNLC were immunostained with the primary antibodies, incubated with the relevant secondary antibody conjugated with FITC and counterstained with propidium iodide. **A–C** Immunostaining of Olig2 (motor neuron progenitor marker). **D–F** Immunostaining of ISLET1 (motor neuron precursor marker). **G–I** Immunostaining of HB9 (marker for the differentiated motor neuron). **J–L** Immunostaining of Chat (choline acetyl transferase: marker for the differentiated neurons). **M–O** Immunostaining of Map2 (marker for neurons) (*scale bar* = 100 μm, all)
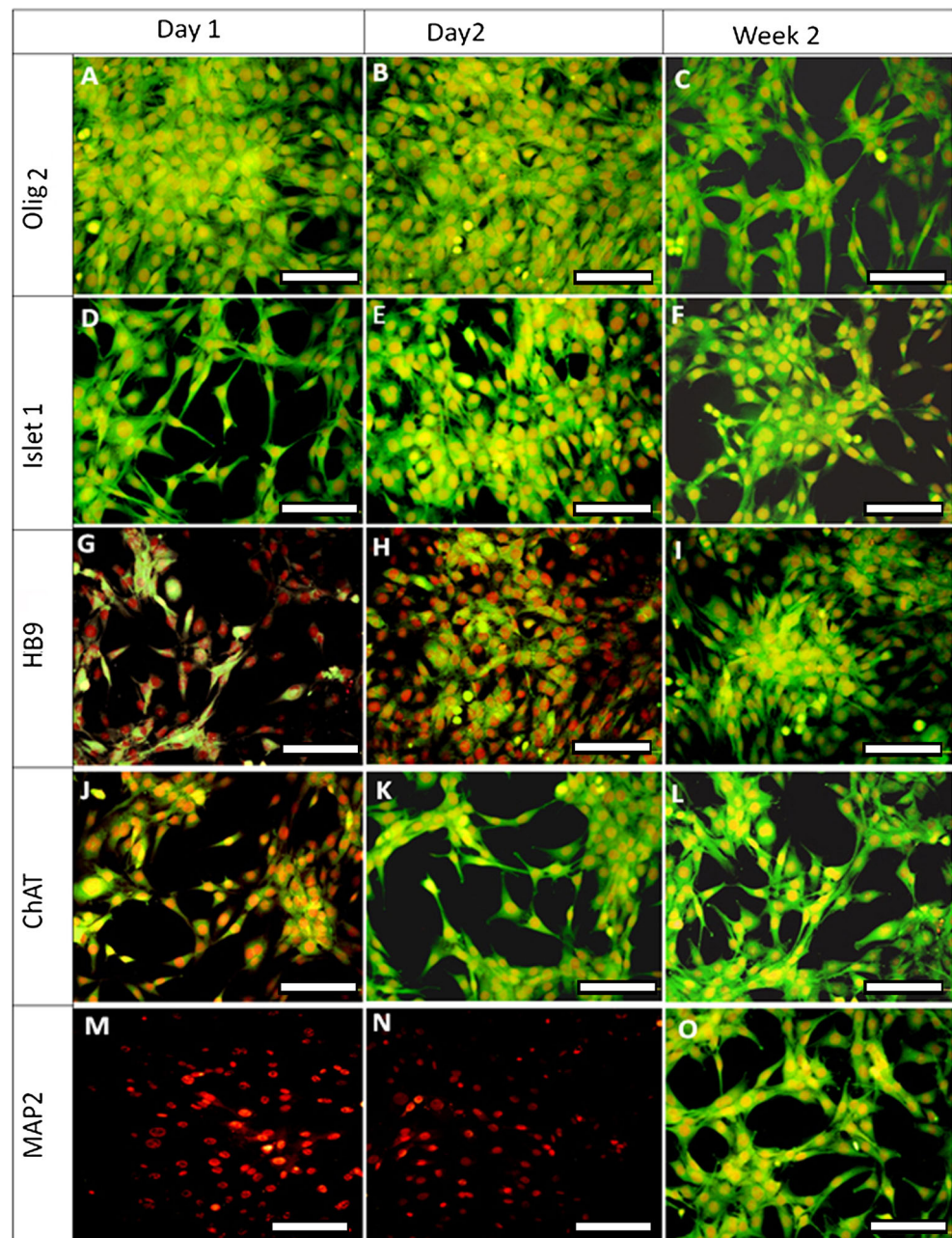
in vitro co-culture system. They could release synaptic vesicles upon stimulation, associated with membrane depolarization and intracellular calcium ion shift.

Differential gene expression of neurotrophins and their receptors in transdifferentiation of bone marrow stromal cells was documented (Yaghoobi and Mowla 2006), so is the differential expression of transcription factors in transdifferentiating ADSC (Cardozo et al. 2010). A temporal gradient in the transcription factor expression (Shh) of differentiation in the central nervous system was documented (Dessaud et al. 2007). In this study, a temporal

gradient in the expression of the transcription factors ISLET1, Olig2, and HB9 in the transdifferentiating ADSC into MNLC have been noticed, which agrees with earlier investigations (Miles et al. 2004). Furthermore, the quantitative immunocytochemical study shows that the highest expression of Olig2 was at day 1, and then it declined. Conversely, the expression of HB9 and Chat was low, and then it increased, which is consistent with previous findings (Yoo et al. 2013). The expression of ISLET1, which was highest at day 2, is consistent with the results of others (Hu and Zhang 2010). On the other hand, the motor neurons
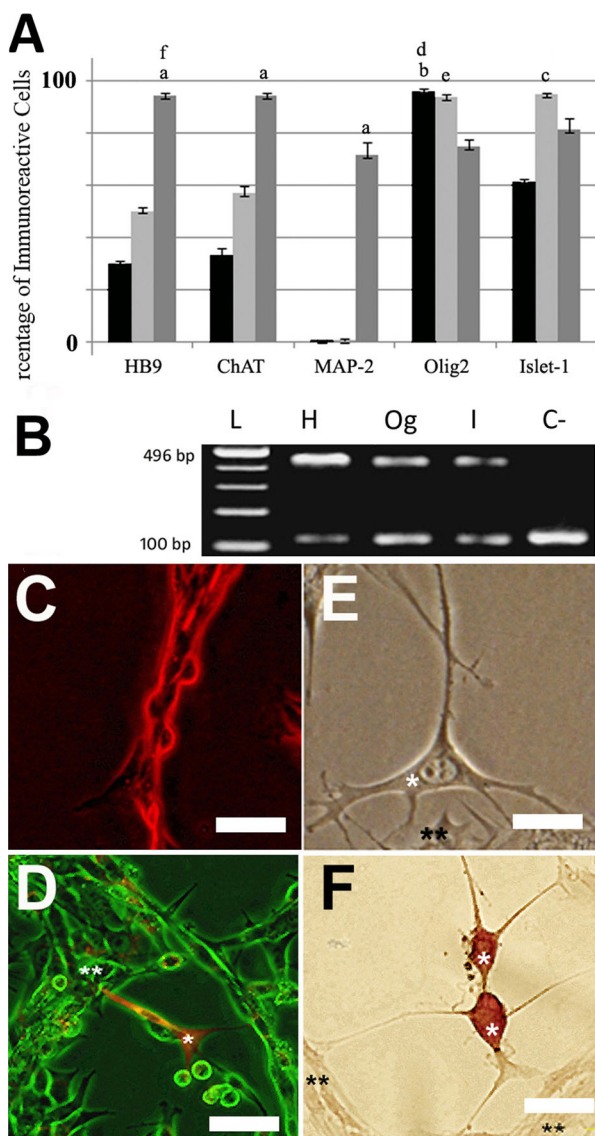
Fig. 4 Characterization of the motor neuron-like cells (MNLC) by quantitative evaluation of the immunoreactivity to their markers, and the electrophoresis results of the reverse transcription polymerase chain reaction (RT-PCR) of MNLC and their co-culturing with myotubes. **A** Histogram of the percentages of immunoreactive cells (motor neuron-like cells: MNLC) to Map2, choline acetyl transferase (Chat), ISLET1, Olig2, and HB9 at day 1, day 2, and 2 weeks (*black*, *light gray*, and *dark gray columns*, respectively). *a* Statistically different from day 2 and 2 weeks, *b* statistically different from 2 weeks, *c* statistically different from day 1 and 2 weeks, *d* significantly higher than the other markers expressed at day 1, *e* significantly higher than the other markers expressed at day 2 except ISLET1, and *e* significantly higher than the other markers expressed at 2 weeks except Chat. **B** Electropherogram of RT-PCR of MNLC and the fragments of RT-PCR for HB9 (H), Olig2 (Og), ISLET1 (I), C-(negative control: with cDNA), and L (DNA ladder). **C** Photomicrograph of a myotube stained with PKh 26 fluorochrome. **D** Myotube stained with PKh 67 and co-cultured with the induced motor neuron-like cells (MNLC) stained with PKh 26. **E** Phase contrast photomicrograph of myotubes co-cultured with the induced MNLC. **F** Myotube co-cultured with the induced motor neuron-like cells stained with Cresyl violet. ****Myotubes** and ***MNLC**

expressed Map2, HB9, and Chat after 4 weeks (Lee et al. 2014), whereas in this study, Olig2, ISLET1, HB9, Map2, and Chat were expressed after 2 weeks. Gou et al. (2010) induced human fetal cell line into motor neurons for 6 days, and only 20 % of the motor neurons expressed HB9, ISLET1 and Chat, while in this study, after 1 week of induction, we noticed that the percentages of the markers were 45, 58, 2, 97, and 97 %, for HB9, Chat, Map2, Olig2, and ISLET1, respectively.

The efficiency of MNLC generation from adult stem cells that we obtained is 95 ± 1.4 % (mean ± SEM), and some investigators reported it from ESCs to be 51 % (Wu et al. 2012) or 75 % (Su et al. 2012). Comparing these results with our findings indicates that we obtained higher efficiency by transdifferentiating ADSC into neurosphere, and generating NS-derived NSC, which were used for producing MNLC.

The results of this multistep protocol are consistent with the finding of a former study that applied a two-step technique using preinduction–induction protocol, where the preinducers were a cocktail of chemicals (isobutyl-methylxanthine and β-mercaptoethanol) with fibroblast growth factor 2 and B27 supplement, whereas the induction stage consisted of B27, RA and Shh followed by B27, vitamin C, BDNF and GDNF, the efficiency was 65 % (Liqing et al. 2011), however, the use of β-mercaptoethanol was reported to cause cell shrinkage and death (Ghorbanian et al. 2010). Thus, the combination of Shh and RA with BDNF, GDNF, CNTF, and NT-3 could cause either additive or synergistic mode of induction (Zurn et al. 1996). In a study, a multistep method was applied in order to induce amniotic-derived mesenchyme stem cells into motor neuron precursor cells by sequential incubations with DMEM/F12, 10 % fetal calf serum and 20 µg/l bFGF; DMEM/F12, 20 g/l B27 and 20 µg/l bFGF; DMEM/F12, 10^{-3} mM/l retinoic acid, 20 g/l B27 and 20 ng/ml β-NGF; and DMEM/F12, 10 % fetal calf serum and 20 µg/l bFGF; however, the source of the cells was allogenic (Hu et al. 2013). Other multistep protocols were used in inducing embryonic stem cells (Wichterle and Peljto 2008) and iPSC (Petros et al. 2011). The transdifferentiation of fibroblast into neuronal phenotype could be reverted into fibroblast (Graf 2011); moreover, mesenchymal stem cells could be reverted to a primitive stem cell population (Rui et al. 2015). The neurosphere culture medium was suggested to be selective for the growth of the cells that form the NS (Aleksandrova et al. 2002; Monni et al. 2011) and contribute to the transplant stability (Joo et al. 2012). Moreover, the transdifferentiated MNLC were derived from NSC, which were immunoreactive to nestin, a marker for neural progenitor cells; however, the motor neuron derived from iPSC was characterized by direct transdifferentiation without intermediary progenitors (no immunoreactivity to

Fig. 5 Release of the vesicles in motor neuron-like cells which are stained with lipophilic fluorochrome (FM1-43) and synaptic vesicles specific protein immunostaining (synaptophysin). **A** Phase contrast of the field used for the staining of the motoneuron-like cells with FM1-43. **B** Staining of the MNLC with FM1-43. **C** Destaining of the MNLC upon stimulation with high concentration of potassium chloride. **D** The curve fitting of the normalized mean gray level values at 10 min intervals (each minute one photograph); the curve fitting shows an exponential decay model. **E** MNLC with double labeling; they were stained with FM1-43, and then immunostained with anti-synaptophysin primary antibody and incubated with a secondary antibody conjugated with FITC. *Arrowheads* indicate double-stained synaptic vesicles located at the periphery. *Empty arrowhead* indicates vesicles present at the contact between the cell extensions and the body of the cells. *Arrows* indicate synaptic vesicles distributed in the cytoplasm of the MNLC (*scale bar* **A–C** = 20 μm and **E** = 50 μm)
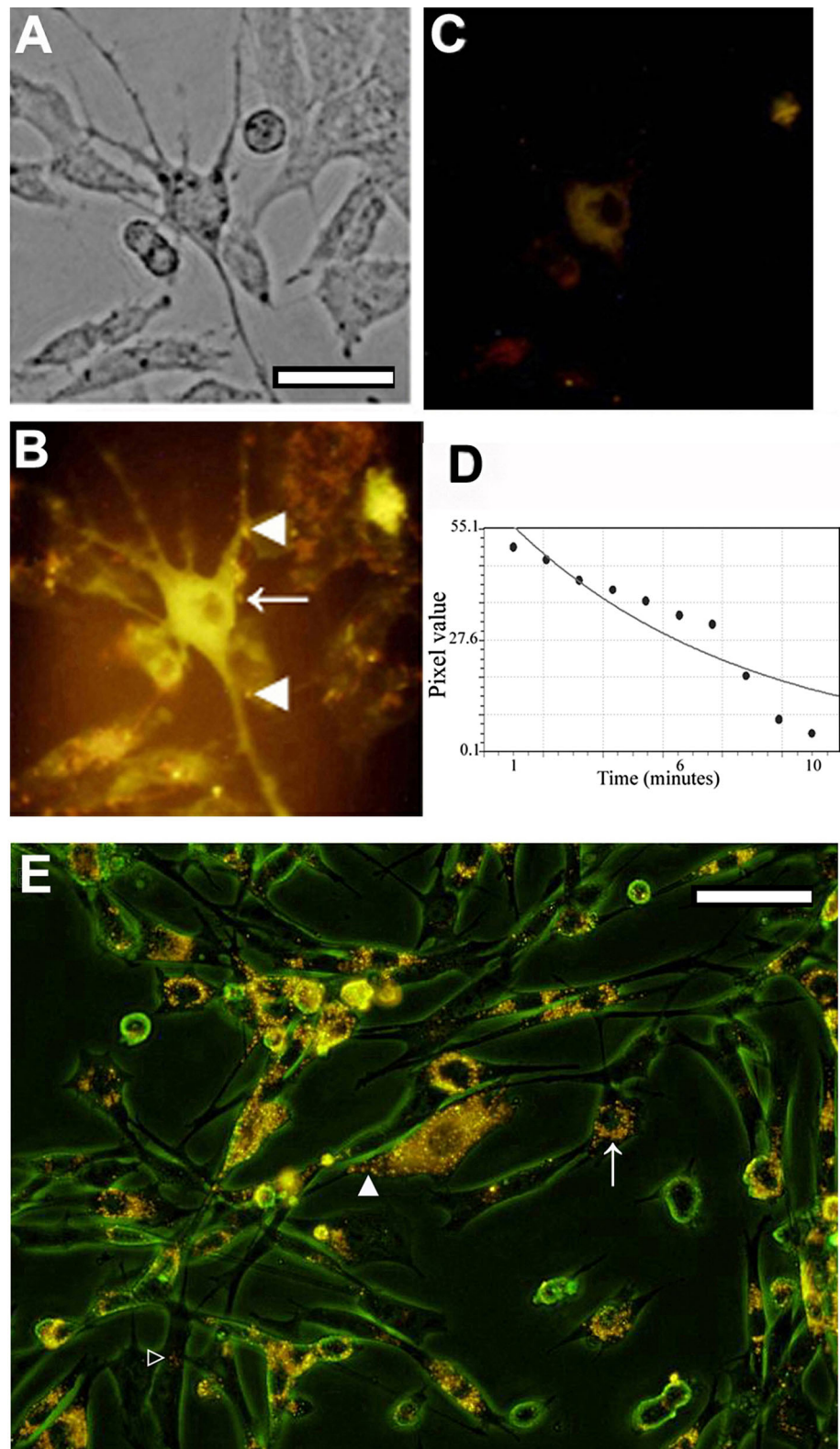
nestin) (Son et al. 2011). The multistep transdifferentiation achieved in this study is characterized by intermediary nestin-immunoreactive cells, which was considered as a lineage reprogramming type (Zhou and Melton 2008),

and this type is characterized by low tumorigenesis risk and increased transdifferentiation efficiency (Asuelime and Shi 2012). We also achieved a stepwise route (indirect) for transdifferentiation, which was mentioned as a
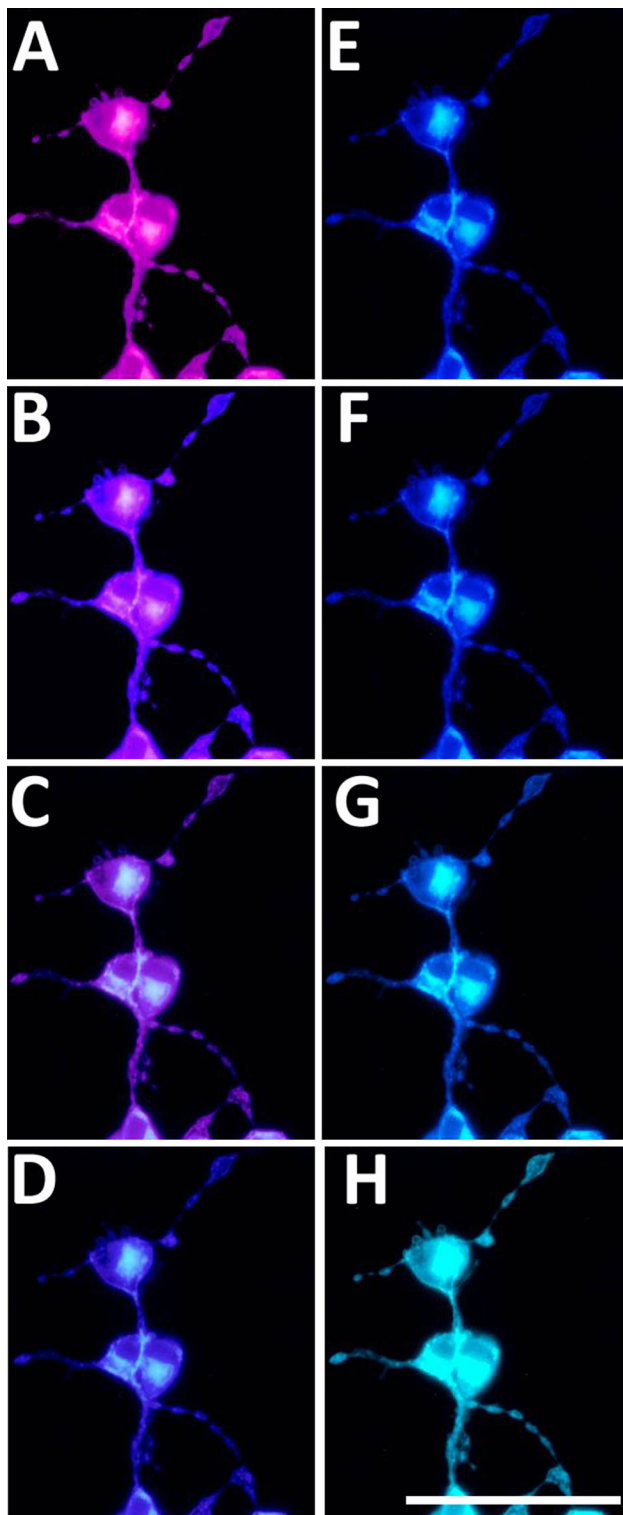
Fig. 6 Staining of the motor neuron-like cells with calcium indicator (Fluo-4 NW). **A** Staining of the motor neuron-like cells with Fluo-4 NW followed by their stimulation, **B–H** Images of the same field photographed serially, which show changes in the color of the cells resulted from a shift in the intracellular Ca^{2+} concentration (*scale bar* **F–K** = 50 μm)

natural transdifferentiation pathway (de Peppo and Marolt 2012).

The synaptic vesicle release is consistent with our previous investigation and has the same monoexponential decay model (Abdanipour and Tiraihi 2012). Some researchers reported an exponential decay pattern in synaptic release (Bamford et al. 2004). The intercept of the fitted nonlinear curve in this study is lower, and the release rate is slower than the previous work, where the binding of fluorochrome to the synaptic vesicles was higher due to their higher density (the intercept was about 150), while the slower release of synaptic vesicles in response to chloride ion stimulation indicates the immaturity of the induced motor neurons in this study compared with the previous study (the rate was 1.4), and this is consistent with findings (Griesinger et al. 2002) that reported closer value for the rate of synaptic release or depolarization of the basal membrane of the inner hair cells. The immaturity of the neurons can be advantageous for transplantation therapy (Naghdi et al. 2009). The colocalized FM1-43 fluorochrome with synaptophysin immunostaining shows that the distribution of synaptic vesicles was at the neuronal extension as well as the periphery of the neuron soma, which was at the same location of the recycled vesicles. The immunostaining of synaptophysin was reported to be correlated with the synaptic release (Staple et al. 1997), where FM1-43 incorporated with the presynaptic sites (Henkel et al. 1996). In this study, we have used voltage-sensitive dyes (RH795) in evaluating the action potential of the cells (Chemla and Chavane 2010), and the electrical activity in the membrane can be detected with VSD, which was documented to be comparable with the patch clamp technique, while membrane depolarization could be monitored in large population of cells in addition to its accuracy and quickness (Leao et al. 2010). Likewise, the calcium indicator was used in evaluating the intracellular calcium ion shift following stimulation of the cells (Sudhof 2012), and in this study, Fluo-4 NW has been used, and the level of calcium increased following stimulation where the membrane depolarized, activating voltage-sensitive calcium channels (Nakanishi and Okazawa 2006), and this finding is consistent with previous reports (Apati et al. 2013). One of the main advantages of production of MNLC with these activities is potential use of these cells in ALS cell therapy, although cell therapy of ALS can be an option for improving the quality of life for the patients (Gonzalez-Garza et al. 2013), there are difficulties such as proper timing of the transplant for engraftment and finding a proper window for re-establishing synaptic connections (Lepore and Maragakis 2007).
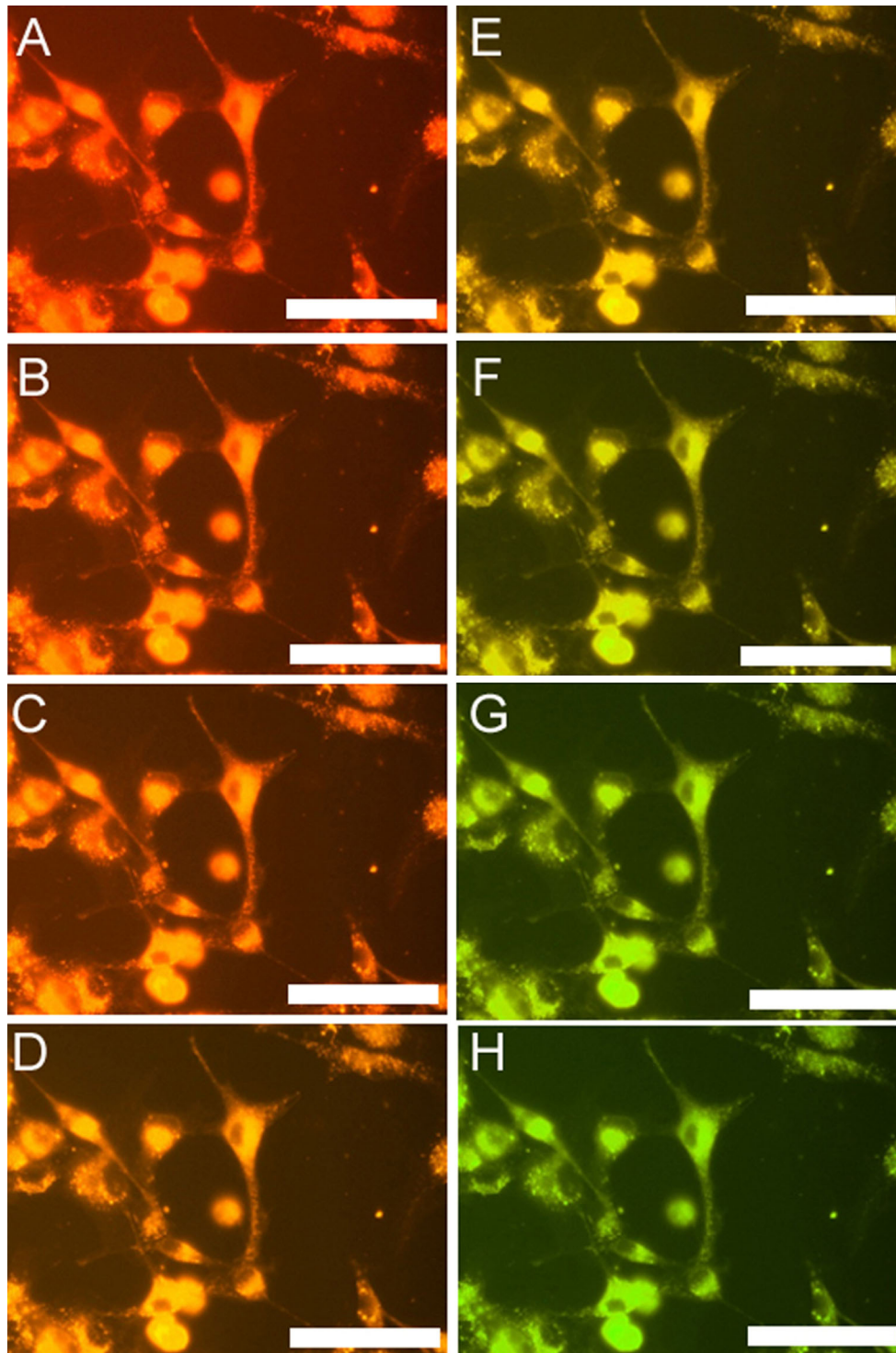
Fig. 7 Staining of the motor neuron-like cells with voltage-sensitive dye (RH795). **A** Staining of the motor neuron-like cells with RH795 followed by their stimulation, **B**–**H** Images of the same field photographed serially, which show changes in the color of the cells resulted from a shift in the membrane depolarization and repolarization (*scale bar* **F**–**K** = 65 μm)

References

Abdanipour A, Tiraihi T (2012) Induction of adipose-derived stem cell into motoneuron-like cells using selegiline as preinducer. Brain Res 1440:23–33. doi:10.1016/j.brainres.2011.12.051

Aleksandrova MA, Saburina IN, Poltavtseva RA, Revishchin AV, Korochkin LI, Sukhikh GT (2002) Behavior of human neural progenitor cells transplanted to rat brain. Brain Res Dev Brain Res 134(1–2):143–148

Apati A, Paszty K, Hegedus L, Kolacsek O, Orban TI, Erdei Z, Szebenyi K, Pentek A, Enyedi A, Sarkadi B (2013) Characterization of calcium signals in human embryonic stem cells and in their differentiated offspring by a stably integrated calcium indicator protein. Cell Signal 25(4):752–759. doi:10.1016/j.cellsig.2012.12.024

Asuelime GE, Shi Y (2012) A case of cellular alchemy: lineage reprogramming and its potential in regenerative medicine. J Mol Cell Biol 4(4):190–196. doi:10.1093/jmcb/mjs005

Bamford NS, Robinson S, Palmiter RD, Joyce JA, Moore C, Meshul CK (2004) Dopamine modulates release from corticostriatal terminals. J Neurosci 24(43):9541–9552. doi:10.1523/jneurosci.2891-04.2004

Baptista LS, Silva KR, Pedrosa CS, Amaral RJ, Belizario JV, Borojevic R, Granjeiro JM (2013) Bioengineered cartilage in a scaffold-free method by human cartilage-derived progenitor cells: a comparison with human adipose-derived mesenchymal stromal cells. Artif Organs 37(12):1068–1075. doi:10.1111/aor.12121

Bieberich E, Anthony GE (2004) Neuronal differentiation and synapse formation of PC12 and embryonic stem cells on interdigitated microelectrode arrays: contact structures for neuron-to-electrode signal transmission (NEST). Biosens Bioelectron 19(8):923–931

Canepari M, Zecevic D (2010) Membrane potential imaging in the nervous system: methods and applications. Springer, New York

Cardozo A, Ielpi M, Gomez D, Argibay P (2010) Differential expression of Shh and BMP signaling in the potential conversion of human adipose tissue stem cells into neuron-like cells in vitro. Gene Expr 14(6):307–319

Chemla S, Chavane F (2010) Voltage-sensitive dye imaging: technique review and models. J Physiol Paris 104(1–2):40–50. doi:10.1016/j.jphysparis.2009.11.009

Darabi S, Tiraihi T, Ruintan A, Abbaszadeh HA, Delshad A, Taheri T (2013) Polarized neural stem cells derived from adult bone marrow stromal cells develop a rosette-like structure. Vitro Cell Dev Biol Anim 49(8):638–652. doi:10.1007/s11626-013-9628-y

Dawitz J, Kroon T, Hjorth JJ, Meredith RM (2011) Functional calcium imaging in developing cortical networks. J Vis Exp. doi:10.3791/3550

de Peppo GM, Marolt D (2012) State of the art in stem cell research: human embryonic stem cells, induced pluripotent stem cells, and transdifferentiation. J Blood Transfus 2012:317632. doi:10.1155/2012/317632

Dessaud E, Yang LL, Hill K, Cox B, Ulloa F, Ribeiro A, Mynett A, Novitch BG, Briscoe J (2007) Interpretation of the sonic hedgehog morphogen gradient by a temporal adaptation mechanism. Nature 450(7170):717–720. doi:10.1038/nature06347

Gharibani PM, Tiraihi T, Arabkheradmand J (2010) In vitro differentiation of GABAergic cells from bone marrow stromal cells using potassium chloride as inducer. Restor Neurol Neurosci 28(3):367–377. doi:10.3233/rnn-2010-0539

Ghorbanian MT, Tiraihi T, Mesbah-Namin SA, Fathollahi Y (2010) Selegiline is an efficient and potent inducer for bone marrow stromal cell differentiation into neuronal phenotype. Neurol Res 32(2):185–193. doi:10.1179/174313209x409016

Gonzalez-Garza MT, Martinez HR, Caro-Osorio E, Cruz-Vega DE, Hernandez-Torre M, Moreno-Cuevas JE (2013) Differentiation of CD133+stem cells from amyotrophic lateral sclerosis patients into preneuron cells. Stem Cells Transl Med 2(2):129–135. doi:10.5966/sctm.2012-0077

Graf T (2011) Historical origins of transdifferentiation and reprogramming. Cell Stem Cell 9(6):504–516. doi:10.1016/j.stem.2011.11.012

Griesinger CB, Richards CD, Ashmore JF (2002) Fm1-43 reveals membrane recycling in adult inner hair cells of the mammalian cochlea. J Neurosci 22(10):3939–3952.

Guo X, Johe K, Molnar P, Davis H, Hickman J (2010) Characterization of a human fetal spinal cord stem cell line, NSI-566RSC, and its induction to functional motoneurons. J Tissue Eng Regen Med 4(3):181–193. doi:10.1002/term.223

Henkel AW, Lubke J, Betz WJ (1996) FM1-43 dye ultrastructural localization in and release from frog motor nerve terminals. Proc Natl Acad Sci USA 93(5):1918–1923

Hester ME, Murtha MJ, Song S, Rao M, Miranda CJ, Meyer K, Tian J, Boulting G, Schaffer DV, Zhu MX (2011) Rapid and efficient generation of functional motor neurons from human pluripotent stem cells using gene delivered transcription factor codes. Mol Ther 19(10):1905–1912

Hu BY, Zhang SC (2010) Directed differentiation of neural-stem cells and subtype-specific neurons from hESCs. Methods Mol Biol 636:123–137. doi:10.1007/978-1-60761-691-7_8

Hu W, Guan FX, Li Y, Tang YJ, Yang F, Yang B (2013) New methods for inducing the differentiation of amniotic-derived mesenchymal stem cells into motor neuron precursor cells. Tissue Cell 45(5):295–305. doi:10.1016/j.tice.2013.03.002

Joo KM, Jin J, Kang BG, Lee SJ, Kim KH, Yang H, Lee Y-A, Cho YJ, Im Y-S, Lee D-S (2012) Trans-differentiation of neural stem cells: a therapeutic mechanism against the radiation induced brain damage. PLoS ONE 7(2):e25936

Kokai LE, Rubin JP, Marra KG (2005) The potential of adipose-derived adult stem cells as a source of neuronal progenitor cells. Plast Reconstr Surg 116(5):1453–1460

Krabbe C, Zimmer J, Meyer M (2005) Neural transdifferentiation of mesenchymal stem cells: a critical review. APMIS 113(11–12):831–844. doi:10.1111/j.1600-0463.2005.apm_3061.x

Leao RN, Reis A, Emirandetti A, Lewicka M, Hermanson O, Fisahn A (2010) A voltage-sensitive dye-based assay for the identification of differentiated neurons derived from embryonic neural stem cell cultures. PLoS ONE 5(11):e13833. doi:10.1371/journal.pone.0013833

Lee HJ, Kim KS, Ahn J, Bae HM, Lim I, Kim SU (2014) Human motor neurons generated from neural stem cells delay clinical onset and prolong life in ALS mouse model. PLoS ONE 9(5):e97518. doi:10.1371/journal.pone.0097518

Lepore AC, Maragakis NJ (2007) Targeted stem cell transplantation strategies in ALS. Neurochem Int 50(7–8):966–975. doi:10.1016/j.neuint.2006.09.005

Liqing Y, Jia G, Jiqing C, Ran G, Fei C, Jie K, Yanyun W, Cheng Z (2011) Directed differentiation of motor neuron cell-like cells from human adipose-derived stem cells in vitro. NeuroReport 22(8):370–373. doi:10.1097/WNR.0b013e3283469615

Miles GB, Yohn DC, Wichterle H, Jessell TM, Rafuse VF, Brownstone RM (2004) Functional properties of motoneurons

derived from mouse embryonic stem cells. J Neurosci 24(36):7848–7858. doi:10.1523/jneurosci.1972-04.2004

Mirakhori F, Zeynali B, Salekdeh GH, Baharvand H (2014) Induced neural lineage cells as repair kits: so close, yet so far away. J Cell Physiol 229(6):728–742. doi:10.1002/jcp.24509

Mohammad-Gharibani P, Tiraihi T, Mesbah-Namin SA, Arabkheradmand J, Kazemi H (2012) Induction of bone marrow stromal cells into GABAergic neuronal phenotype using creatine as inducer. Restor Neurol Neurosci 30(6):511–525. doi:10.3233/rnn-2012-100155

Monni E, Congiu T, Massa D, Nat R, Diana A (2011) Human neurospheres: from stained sections to three-dimensional assembly. Transl Neurosci 2(1):43–48

Naghdi M, Tiraihi T, Namin SA, Arabkheradmand J (2009) Transdifferentiation of bone marrow stromal cells into cholinergic neuronal phenotype: a potential source for cell therapy in spinal cord injury. Cytotherapy 11(2):137–152. doi:10.1080/14653240802716582

Nakanishi S, Okazawa M (2006) Membrane potential-regulated Ca2 + signalling in development and maturation of mammalian cerebellar granule cells. J Physiol 575(Pt 2):389–395. doi:10.1113/jphysiol.2006.113340

Nizzardo M, Simone C, Falcone M, Locatelli F, Riboldi G, Comi GP, Corti S (2010) Human motor neuron generation from embryonic stem cells and induced pluripotent stem cells. Cell Mol Life Sci 67(22):3837–3847. doi:10.1007/s00018-010-0463-y

Petros TJ, Tyson JA, Anderson SA (2011) Pluripotent stem cells for the study of CNS development. Front Mol Neurosci 4:30. doi:10.3389/fnmol.2011.00030

Rui Y, Xu L, Chen R, Zhang T, Lin S, Hou Y, Liu Y, Meng F, Liu Z, Ni M, Tsang KS, Yang F, Wang C, Chan HC, Jiang X, Li G (2015) Epigenetic memory gained by priming with osteogenic induction medium improves osteogenesis and other properties of mesenchymal stem cells. Sci Rep 5:11056. doi:10.1038/srep11056

Silani V, Fogh I, Ratti A, Sassone J, Ciammola A, Cova L (2002) Stem cells in the treatment of amyotrophic lateral sclerosis (ALS). Amyotroph Lateral Scler Other Motor Neuron Disord 3(4):173–181

Son EY, Ichida JK, Wainger BJ, Toma JS, Rafuse VF, Woolf CJ, Eggan K (2011) Conversion of mouse and human fibroblasts into functional spinal motor neurons. Cell Stem Cell 9(3):205–218. doi:10.1016/j.stem.2011.07.014

Staple JK, Osen-Sand A, Benfenati F, Pich EM, Catsicas S (1997) Molecular and functional diversity at synapses of individual neurons in vitro. Eur J Neurosci 9(4):721–731

Su H, Zhang W, Yang X, Qin D, Sang Y, Wu C, Wong WM, Yuan Q, So KF, Wu W (2012) Neural progenitor cells generate motoneuron-like cells to form functional connections with target muscles after transplantation into the musculocutaneous nerve. Cell Transplant 21(12):2651–2663. doi:10.3727/096368912x654975

Sudhof TC (2012) Calcium control of neurotransmitter release. Cold Spring Harb Perspect Biol 4(1):a011353. doi:10.1101/cshperspect.a011353

Wichterle H, Peljto M (2008) Differentiation of mouse embryonic stem cells to spinal motor neurons. Curr Protoc Stem Cell Biol Chapter 1 Unit 1H 1 1-1H 1 9. doi:10.1002/9780470151808.sc01h01s5

Wu CY, Whye D, Mason RW, Wang W (2012) Efficient differentiation of mouse embryonic stem cells into motor neurons. J Vis Exp 64:e3813. doi:10.3791/3813

Yaghoobi MM, Mowla SJ (2006) Differential gene expression pattern of neurotrophins and their receptors during neuronal differentiation of rat bone marrow stromal cells. Neurosci Lett 397(1–2):149–154. doi:10.1016/j.neulet.2005.12.009

Yoo J, Kim HS, Hwang DY (2013) Stem cells as promising therapeutic options for neurological disorders. J Cell Biochem 114(4):743–753. doi:10.1002/jcb.24427

Zhou Q, Melton DA (2008) Extreme makeover: converting one cell into another. Cell Stem Cell 3(4):382–388. doi:10.1016/j.stem.2008.09.015

Zurn AD, Winkel L, Menoud A, Djabali K, Aebischer P (1996) Combined effects of GDNF, BDNF, and CNTF on motoneuron differentiation in vitro. J Neurosci Res 44(2):133–141. doi:10.1002/(SICI)1097-4547(19960415)44:2<133:AID-JNR5>3.0.CO;2-E